Smart Antenna Performance and Complexity for Estimated Rician Fading with Correlated Azimuth Spread and K-Factor

Constantin Siriteanu, Yoshikazu Miyanaga, and Steven D. Blostein

***Abstract*—This work shows that the full performance permitted by the Rician fading radio channel at a smart antenna receiver with imperfect channel state information is achieved with maximal-ratio eigencombining (MREC) for much lower complexity (i.e., baseband power consumption) than with conventional maximal-ratio combining. Furthermore, it shows that unrealistic assumptions about the channel fading (Rayleigh, Rician with typical K value) produce not only several-dB performance estimation inaccuracies, but also up to 50% processing cost estimation inaccuracies. These results are obtained by deriving a new average (over the noise and fading) error probability expression for MREC, and then averaging it numerically over lognormal azimuth spread and K-factor distributions recently reported from measurements. A MREC adaptation criterion earlier proposed for Rayleigh fading is generalized to Rician fading and demonstrates an excellent dimension-reduction capability, for more power-efficient smart antennas.**

***Index Terms*—Azimuth spread, Rician fading, eigencombining.**

I. INTRODUCTION

This paper sets out to compare smart antenna performance and numerical complexity (which translates into baseband hardware requirements and power consumption) for several

1) Combining methods [1]:
   - Maximal-ratio eigencombining (MREC)
   - Maximal-ratio combining (MRC)
   - Statistical beamforming (BF),
2) Channel state information (CSI) estimation methods [2]:
   - Optimum and suboptimum fading gain estimation,
3) Channel fading and parameter models [3] [4] [5]:
   - Rician fading and Rayleigh fading,
   - Lognormal, correlated azimuth spread (AS) and K-factor, and nonrandom AS and K.

This analysis is necessary because, in practice, conventional combiners such as MRC and BF do not adjust processing requirements to the channel condition. On the other hand, MREC (which is a superset of MRC and BF) can process only the dominant eigenvectors [1]. Furthermore, CSI estimation is imperfect and consumes significant hardware resources and power for MRC in Rayleigh fading [1] [6]. Finally, the effect of realistic Rician fading with large (negative) AS – K correlation [5] on smart antenna performance and baseband processing complexity has not been investigated by others.

To undertake the analysis we derive a new expression for the MREC average error probability (AEP — over noise and fading) for imperfect CSI, Rician fading, and any AS and K-factor values. This expression is then averaged numerically over AS and K distributions reported from measurements [5]. A criterion for MREC adaptation to actual channel condition is also proposed, to minimize the dimension of the channel estimation and signal combining problem.

Throughout this paper, numerical complexity refers to the number of multiplications required for combining, estimating the fading gains (i.e., the CSI), and estimating the channel eigenstructure [1] [7]. Computational complexity translates into hardware requirements and power consumption, as shown for FPGA-based MREC, MRC, and BF implementations and Rayleigh fading in [6].

Using the performance and complexity evaluation approaches described above, we first show, for Rician fading, estimated CSI, and random AS and K, that: 1) unlike BF and MRC, MREC can yield a channel-driven performance–complexity trade-off; 2) the MREC decorrelating step simplifies optimum CSI estimation tremendously. These results are consistent with our previous results for Rayleigh fading [1]. They suggest that we should deploy MREC if we want 'green' smart antennas, which achieve the optimum performance permitted by the channel for minimum baseband hardware requirements and power consumption.

Secondly, for adaptive MREC, the Rayleigh fading assumption is found to significantly underestimate performance and overestimate complexity compared to the measurement-supported Rician fading model with correlated AS and K. On the other hand, Rician fading with K set to typical value is found to significantly overestimate performance and underestimate complexity. Then, increasing AS – K correlation is shown to yield improving performance indications and no significant complexity increase.

Section II of this paper presents the signal, AS, and K-factor models. Section III describes MREC, its relationships with MRC and BF, as well as adaptive order selection, for Rician fading and estimated CSI. Finally, Section IV presents numerical results that support our claims.

Constantin (Costi) Siriteanu is GCOE Assistant Professor, Graduate School of Information Science and Technology, Hokkaido University, Sapporo, Japan. E-mail: costi@icn.ist.hokudai.ac.jp

Yoshikazu Miyanaga is Professor, Graduate School of Information Science and Technology Hokkaido University, Sapporo, Japan. E-mail: miya@ist.hokudai.ac.jp

Steven D. Blostein is Professor, Department of Electrical and Computer Engineering, Queen's University, Kingston, Canada. E-mail: steven.blostein@queensu.ca

978-1-4244-6878-2/10/$26.00 ©2010 IEEE

II. Signal, Channel, and Noise Models

A. Received Signal Model

A single-antenna mobile station transmits signal through a frequency-flat Rician fading channel. At an L-element base-station antenna array the received signal vector after demodulation, matched-filtering, and symbol-rate sampling is [1]

$$\widetilde{\mathbf{y}} = \sqrt{E_\mathrm{s}}\, b\, \widetilde{\mathbf{h}} + \widetilde{\mathbf{n}} \tag{1}$$

where E_s is the energy transmitted per symbol, and the random transmitted symbol b is drawn from an M-PSK constellation with unit amplitude. The channel fading and receiver noise vectors, $\widetilde{\mathbf{h}}$ and $\widetilde{\mathbf{n}}$, are assumed to be mutually uncorrelated, circularly-symmetric, complex-valued, random Gaussian vectors [3, p. 39], described by $\widetilde{\mathbf{h}} \sim \mathcal{N}_c(\widetilde{\mathbf{h}}_\mathrm{d}, \mathbf{R}_{\widetilde{\mathbf{h}}})$ and $\widetilde{\mathbf{n}} \sim \mathcal{N}_c(\mathbf{0}, N_0\,\mathbf{I})$.

The Rician K-factor is the ratio of the powers in the deterministic part (i.e., the mean) and the random part of the channel vector [3]. Then, the channel vector can be written as:

$$\widetilde{\mathbf{h}} = \sqrt{\frac{K}{K+1}}\,\widetilde{\mathbf{h}}_\mathrm{d,n} + \sqrt{\frac{1}{K+1}}\,\widetilde{\mathbf{h}}_\mathrm{r,n}, \tag{2}$$

where $\widetilde{\mathbf{h}}_\mathrm{d,n}$ is the 'normalized' deterministic part of $\widetilde{\mathbf{h}}$, i.e., we assume that its elements have the property $|\widetilde{h}_{\mathrm{d,n},i}| = 1$, and $\widetilde{\mathbf{h}}_\mathrm{r,n}$ is the 'normalized' random part of $\widetilde{\mathbf{h}}$, i.e., we assume that $E\{|\widetilde{h}_{\mathrm{r,n},i}|^2\} = 1$. Then, $E\{|h_i|^2\} = 1$, and the average bit-SNR is given by $\gamma_\mathrm{b} = \frac{1}{\log_2 M}\frac{E_\mathrm{s}}{N_0}E\{|h_i|^2\} = \frac{1}{\log_2 M}\frac{E_\mathrm{s}}{N_0}$.

The deterministic channel gain part is:

$$E\{\widetilde{\mathbf{h}}\} = \widetilde{\mathbf{h}}_\mathrm{d} = \sqrt{\frac{K}{K+1}}\,\widetilde{\mathbf{h}}_\mathrm{d,n}. \tag{3}$$

The distribution of the normalized random part is completely described by its correlation matrix, $\mathbf{R}_{\widetilde{\mathbf{h}}_\mathrm{r,n}} = E\{\widetilde{\mathbf{h}}_\mathrm{r,n}\,\widetilde{\mathbf{h}}_\mathrm{r,n}^\mathsf{H}\}$. The covariance matrix of the channel gain vector and the correlation matrix of its random part are related as:

$$\mathbf{R}_{\widetilde{\mathbf{h}}} = E\left\{\left(\widetilde{\mathbf{h}} - \widetilde{\mathbf{h}}_\mathrm{d}\right)\left(\widetilde{\mathbf{h}} - \widetilde{\mathbf{h}}_\mathrm{d}\right)^\mathsf{H}\right\} = \frac{1}{K+1}\,\mathbf{R}_{\widetilde{\mathbf{h}}_\mathrm{r,n}}. \tag{4}$$

We will assume that the (real-valued and non-negative) eigenvalues of $\mathbf{R}_{\widetilde{\mathbf{h}}_\mathrm{r,n}}$ are ordered as $\lambda_1 \geq \lambda_2 \geq \ldots \geq \lambda_L \geq 0$. The corresponding, orthonormal, eigenvectors are denoted as $\mathbf{u}_i$, $i = 1:L$. The eigendecomposition of $\mathbf{R}_{\widetilde{\mathbf{h}}_\mathrm{r,n}}$ is then:

$$\mathbf{R}_{\widetilde{\mathbf{h}}_\mathrm{r,n}} = \mathbf{U}_L\mathbf{\Lambda}_L\mathbf{U}_L^H = \sum_{i=1}^{L}\lambda_i\,\mathbf{u}_i\,\mathbf{u}_i^H, \tag{5}$$

where $\mathbf{\Lambda}_L$ and $\mathbf{U}_L$ are, respectively, a diagonal and a unitary matrix formed with the eigenvalues and eigenvectors of $\mathbf{R}_{\widetilde{\mathbf{h}}_\mathrm{r,n}}$.

B. Statistical Models for AS and K

Several authors have shown that the measured K-factor is lognormally distributed [8, Table II]. For a typical scenario, the following K-factor (in dB) model was proposed in [8, Table II]:

$$K_\mathrm{dB} = 7.87\,\psi + 8.53; \quad \psi \sim \mathcal{N}(0,1). \tag{6}$$

On the other hand, signal power arrives with azimuth angle dispersion that is typically modeled by the Laplacian power azimuth spectrum (PAS) [4]. Laplacian PAS is parameterized by the mean angle of arrival (AOA), θ_c, as well as by the AS, which is (approximately) the root second central moment of the PAS. The correlation between two antenna elements can then be computed. For the numerical results shown later a scenario described in [4, Table I] is considered whereby the base-station AS, measured in degrees, is described by lognormal distribution [4, Eqn. (9)]

$$\mathrm{AS} = 10^{0.47\,\chi + 0.74}; \quad \chi \sim \mathcal{N}(0,1). \tag{7}$$

AS samples generated with (7) then yield $\Pr(1^\circ < \mathrm{AS} < 20^\circ) \approx 0.8$ [1], which implies preponderantly-high (over 0.5) antenna correlation values for compact antenna arrays (with unitary normalized inter-element distance, $d_\mathrm{n} = 1$, i.e., physical distance equals half of the carrier wavelength) [1, Fig. 1]. Note that the AS also experiences very slow fluctuations (compared to the Doppler-induced channel gain fluctuation) with the distance traveled by the mobile station [4, Eqn. (14)].

Recent channel measurements and modeling found significant (negative) AS and K correlation. For example, the correlation ρ between ψ and χ has been found to be in the range $[-0.1,\ -0.6]$ in [5, Table 4-5, p. 47]. Therefore, next, we derive an AEP expression for the MREC that we can then numerically average over the above AS and K distributions.

III. MREC, MRC, and BF

A. MREC for Perfect CSI

We summarize below from [1, Section III.A.1] the steps of maximal-ratio eigencombining (MREC) of order $N = 1:L$, denoted hereafter as MREC_N:

(1) The $L \times N$ matrix $\mathbf{U}_N \triangleq [\mathbf{u}_1\ \mathbf{u}_2\ \ldots\ \mathbf{u}_N]$ transforms the signal vector from (1) into

$$\mathbf{y} = \sqrt{E_\mathrm{s}}\,b\,\mathbf{h} + \mathbf{n}, \tag{8}$$

where

$$\mathbf{y} \triangleq \mathbf{U}_N^H\,\widetilde{\mathbf{y}}, \quad \mathbf{h} \triangleq \mathbf{U}_N^H\,\widetilde{\mathbf{h}}, \quad \mathbf{n} \triangleq \mathbf{U}_N^H\,\widetilde{\mathbf{n}}. \tag{9}$$

This is the well-known Karhunen-Loeve Transform (KLT). The elements of the N-dimensional vectors $\mathbf{y}$ and $\mathbf{h}$ are hereafter referred to as *eigenbranches* and *eigengains*, respectively. Our assumptions about the fading and noise imply that:

- $\mathbf{h} \sim \mathcal{N}_c(\mathbf{h}_\mathrm{d}, \frac{1}{K+1}\mathbf{\Lambda}_N)$, where $\mathbf{h}_\mathrm{d} \triangleq \mathbf{U}_N^H\,\widetilde{\mathbf{h}}_\mathrm{d} = \sqrt{\frac{K}{K+1}}\mathbf{U}_N^H\,\widetilde{\mathbf{h}}_\mathrm{d,n}$
- The eigengains are independent
- $\mathbf{n} \sim \mathcal{N}_c(\mathbf{0}, N_0\,\mathbf{I}_N)$.

(2) For perfectly known channel gains (i.e., channel state information — CSI) and eigenstructure, the transformed signal vector is linearly combined, based on the maximal-ratio combining criterion [9], with

$$\mathbf{w}_\mathrm{MREC} = \mathbf{h}. \tag{10}$$

The post-KLT channel vector can be written as:

$$\mathbf{h} = \sqrt{\frac{K}{K+1}}\,\mathbf{h}_{\mathrm{d,n}} + \sqrt{\frac{1}{K+1}}\,\mathbf{h}_{\mathrm{r,n}}, \tag{11}$$

where $\mathbf{h}_{\mathrm{r,n}} \triangleq \mathbf{U}_N^H\,\widetilde{\mathbf{h}}_{\mathrm{r,n}}$. Then, the post-KLT K-factor on the ith eigenbranch, i.e., the ratio of the powers in the deterministic and the random parts, is:

$$K_i = \frac{\frac{K}{K+1}\,|h_{\mathrm{d,n},i}|^2}{\frac{1}{K+1}\,E\{|h_{\mathrm{r,n},i}|^2\}} = K\,\frac{|\mathbf{u}_i^{\mathrm{H}}\,\widetilde{\mathbf{h}}_{\mathrm{d,n}}|^2}{\lambda_i}. \tag{12}$$

B. Exact MREC for Estimated CSI

The analysis below is a generalization to Rician fading and estimated CSI of the analysis for Rayleigh fading and estimated CSI from [1, Section III.D], and of the analysis for Rician fading and perfect CSI from [10, Section III.A]. Hereafter, we assume that CSI is obtained based on pilot-symbol-aided modulation (PSAM) at the transmitter and pilot sample interpolation at the receiver. The SINC PSAM (data-independent, low-complexity, suboptimum) and MMSE PSAM (data-dependent, high-complexity, optimum) estimation methods are described for Rayleigh fading in [2].

1) Optimum Eigencombining — Exact MREC: We describe next a lesser-known, yet optimum, combining method that is difficult to deploy and analyze when deployed pre-KLT, but not so post-KLT.

Recall first that we assume that the deterministic part of the channel eigengain, $\mathbf{h}_{\mathrm{d}}$, is perfectly known. The eigengain vector, $\mathbf{h}$, and its estimate, $\mathbf{g}$, are jointly Gaussian for MMSE and SINC PSAM estimation. Let us denote the mean (i.e., deterministic part) of $\mathbf{g}$ as $\mathbf{g}_{\mathrm{d}}$. Then, the distribution of the eigengain vector, $\mathbf{h}$, conditioned on its estimate, $\mathbf{g}$, is $\mathcal{N}_c(\mathbf{m}, \mathbf{R_e})$, where [1, Section III.D]:

$$\mathbf{m} = \mathbf{h}_{\mathrm{d}} + \mathbf{R}_{\mathbf{hg}}\,\mathbf{R}_{\mathbf{g}}^{-1}\,(\mathbf{g} - \mathbf{g}_{\mathrm{d}}), \tag{13}$$

$$\mathbf{R_e} = \mathbf{R_h} - \mathbf{R}_{\mathbf{hg}}\,\mathbf{R}_{\mathbf{g}}^{-1}\,\mathbf{R}_{\mathbf{gh}}. \tag{14}$$

Then, we can decompose the channel eigengain vector as

$$\mathbf{h} = \mathbf{m} + \mathbf{e}, \quad \mathbf{e} \sim \mathcal{N}_c\,(\mathbf{0}, \mathbf{R_e}), \tag{15}$$

and the post-KLT signal vector from (8) as

$$\mathbf{y} = \sqrt{E_{\mathrm{s}}}\,b\,\mathbf{m} + \boldsymbol{\nu} \sim \mathcal{N}_c(\sqrt{E_{\mathrm{s}}}\,b\,\mathbf{m}, \mathbf{R}_{\boldsymbol{\nu}}) \tag{16}$$

where $\boldsymbol{\nu} \triangleq \sqrt{E_{\mathrm{s}}}\,b\,\mathbf{e} + \mathbf{n}$ compounds the channel estimation impairments and noise, and $\mathbf{R}_{\boldsymbol{\nu}} = E_{\mathrm{s}}\,\mathbf{R_e} + N_0\,\mathbf{I}_N$.

Eigenbranch independence makes the elements of $\mathbf{g}$ independent, and the covariance matrices from (13) and (14) diagonal. Then, the elements of the 'virtual' channel vector $\mathbf{m}$ from (13) and of the covariance matrix $\mathbf{R}_{\boldsymbol{\nu}}$ of the 'virtual' noise vector $\boldsymbol{\nu}$ from (16) can be written, respectively, as:

$$m_i = \sqrt{\frac{K}{K+1}}\,h_{\mathrm{d,n},i} + \sqrt{\frac{\lambda_i}{K+1}}\,\mu_i\,\frac{g_i - g_{\mathrm{d},i}}{\sigma_{g_i}} \tag{17}$$

$$(\mathbf{R}_{\boldsymbol{\nu}})_{i,i} = \frac{1}{K+1}\,E_{\mathrm{s}}\,\lambda_i\,\left(1 - |\mu_i|^2\right) + N_0, \tag{18}$$

where $\sigma_{h_i,g_i} \triangleq E\{(h_i - h_{\mathrm{d},i})\,(g_i - g_{\mathrm{d},i})^*\}$, $\sigma_{g_i}^2 \triangleq E\{|g_i - g_{\mathrm{d},i}|^2\}$, and $\mu_i \triangleq \frac{\sigma_{h_i,g_i}}{\sqrt{\sigma_{h_i}^2\,\sigma_{g_i}^2}} = \sqrt{\frac{K+1}{\lambda_i}}\,\frac{\sigma_{h_i,g_i}}{\sigma_{g_i}}$. The required correlations can be computed for SINC and MMSE PSAM from [2, Tables 2, 3] with λ_i replaced by $\lambda_i/(K+1)$, which is because the work in [2] is for Rayleigh fading.

For (16) the optimum weight vector is

$$\mathbf{w}_{\mathrm{e},N} = \mathbf{R}_{\boldsymbol{\nu}}^{-1}\,\mathbf{m}. \tag{19}$$

Then, the symbol-detection SNR can readily be shown to be

$$\gamma = E_{\mathrm{s}}\sum_{i=1}^{N}\frac{|m_i|^2}{(\mathbf{R}_{\boldsymbol{\nu}})_{i,i}} = \sum_{i=1}^{N}\gamma_i, \tag{20}$$

i.e., the sum of the individual SNRs, which are given by

$$\gamma_i = \frac{E_{\mathrm{s}}\,|m_i|^2}{(\mathbf{R}_{\boldsymbol{\nu}})_{i,i}} = \frac{\frac{E_{\mathrm{s}}}{N_0}\left|\sqrt{K}\,h_{\mathrm{d,n},i} + \sqrt{\lambda_i}\,\mu_i\,\frac{(g_i - g_{\mathrm{d},i})}{\sigma_{g_i}}\right|^2}{\frac{E_{\mathrm{s}}}{N_0}\,\lambda_i\,(1 - |\mu_i|^2) + K + 1}, \tag{21}$$

with average:

$$\Gamma_i = \frac{\frac{E_{\mathrm{s}}}{N_0}\,\lambda_i\,\left(K_i + |\mu_i|^2\right)}{\frac{E_{\mathrm{s}}}{N_0}\,\lambda_i\,(1 - |\mu_i|^2) + K + 1}, \quad i = 1:N. \tag{22}$$

Due to property (20), this optimum combining method has been denoted *exact MREC* [1]. From (19), the exact-MREC weights are:

$$[\mathbf{w}_{\mathrm{e},N}]_i = \frac{m_i}{(\mathbf{R}_{\boldsymbol{\nu}})_{i,i}}, \quad i = 1:N.$$

They require more information and computation than the (more commonly used) *approximate* MREC weights, which are simply $[\mathbf{w}_{\mathrm{a},N}]_i = g_i$, $i = 1:N$ [1]. However, it is shown below that exact-MREC can be analyzed easily (unlike approximate MREC [1]).

2) Exact-MREC Performance Analysis: For the CSI-estimation-error-aware post-KLT signal vector model from (16) the 'virtual' channel eigengain vector $\mathbf{m}$ is described by (17). Then, the 'virtual' K-factor for the ith eigenbranch, i.e., the ratio of the powers in the deterministic and the random parts of m_i, can be written as follows:

$$K_{\mathrm{v},i} = \frac{K\,|h_{\mathrm{d,n},i}|^2}{\lambda_i}\,\frac{1}{|\mu_i|^2} = K_i\,\frac{1}{|\mu_i|^2}. \tag{23}$$

Then, the eigenbranch SNRs from (21) are independent random variables with noncentral χ^2 distributions described by the probability density function [9, Eqn. (2.16), p. 21], and moment generating function [9, Eqn. (2.17), p. 21]

$$M_{\gamma_i}(s) = E\{e^{s\,\gamma_i}\} = \frac{K_{\mathrm{v},i} + 1}{(K_{\mathrm{v},i} + 1) - s\,\Gamma_i}\,e^{\frac{K_{\mathrm{v},i}\,s\,\Gamma_i}{(K_{\mathrm{v},i}+1) - s\,\Gamma_i}}. \tag{24}$$

The exact-MREC symbol-detection SNR, i.e., γ from (20), is the sum of the individual SNRs, which are statistically independent. Then, we can express the symbol AEP based on the method from [9, Chapter 9]. For MREC$_N$ and M-PSK transmitted signals, the symbol error probability conditioned on γ can be written as [9, Eqn. 8.22]

$$P_{e,N}(\gamma) = \frac{1}{\pi}\int_0^{\frac{M-1}{M}\pi}\exp\left\{-\gamma\,\frac{g_{\mathrm{PSK}}}{\sin^2\phi}\right\}d\phi, \tag{25}$$

where $g_{\text{PSK}} = \sin^2 \pi/M$. Then, the AEP is

$$P_{e,N} \triangleq E\{P_{e,N}(\gamma)\} = \frac{1}{\pi} \int_0^{\frac{M-1}{M}\pi} M_\gamma \left(-\frac{g_{\text{PSK}}}{\sin^2 \phi} \right) d\phi, \quad (26)$$

where $M_\gamma(s)$ is the MGF of γ. Using (20) and the independence of γ_i, $i = 1 : N$, (26) becomes

$$P_{e,N} = \frac{1}{\pi} \int_0^{\frac{M-1}{M}\pi} \prod_{i=1}^{N} M_{\gamma_i} \left(-\frac{g_{\text{PSK}}}{\sin^2 \phi} \right) d\phi. \quad (27)$$

This equation and the expression shown above for $M_{\gamma_i}(s)$ yield the symbol-AEP expression for exact MREC$_N$ as

$$P_{e,N} = \frac{1}{\pi} \int_0^{\frac{M-1}{M}\pi} \prod_{i=1}^{N} \frac{(K_{\text{v},i}+1)\, e^{-\frac{K_{\text{v},i} \frac{g_{\text{PSK}}}{\sin^2 \phi} \Gamma_i}{(K_{\text{v},i}+1) + \frac{g_{\text{PSK}}}{\sin^2 \phi} \Gamma_i}}}{(K_{\text{v},i}+1) + \frac{g_{\text{PSK}}}{\sin^2 \phi} \Gamma_i} d\phi, \quad (28)$$

which depends on modulation constellation size, M, MREC order, N, antenna correlation (i.e., also AS), K-factor, as well as estimation method and its parameters. Therefore, (28) suits well our goal of evaluating the effect on performance of the AS – K correlation.

3) Relation with BF and MRC: For $N = 1$, exact MREC becomes exact BF, and then (28) is the BF AEP expression. For $N = L$, exact MREC (i.e., full-MREC) is performance-equivalent to exact MRC because the symbol-detection SNRs are equal. Thus, (28) for full-MREC describes exact-MRC performance. Note that exact-MRC implementation is cumbersome and analysis can be difficult through means other than the equivalence with exact MREC.

4) Relation with Ideal Eigencombining: Perfect CSI implies: $g_i = h_i$, $h_{\text{d},i} = g_{\text{d},i}$, $\sigma_{h_i,g_i} = \sigma^2_{g_i} = \sigma^2_{h_i} = \frac{1}{K+1}\lambda_i$, $\mu_i = 1$, $m_i = h_i$, $K_{\text{v},i} = K_i$, $(\mathbf{R}_{\boldsymbol{\nu}})_{i,i} = N_0$, $[\mathbf{w}_{\text{e},N}]_i = h_i$, $\gamma_i = \frac{E_s}{N_0}|h_i|^2$, and $\Gamma_i = \frac{E_s}{N_0}\lambda_i$. Substituting these specializes (28) as the MREC AEP for perfect CSI [10, Eqn. (15)].

C. Optimum Order Selection for MREC

For Rayleigh fading and the signal model from (8) we previously adapted the MREC order to bit-SNR and AS (assuming eigenvalues ordered decreasingly) using the *bias-variance tradeoff* criterion (BVTC) from [1, Section IV.A]. It balances the loss incurred by removing the weakest $(L - N)$ intended-signal contribution (i.e., *bias*) against the residual-noise contribution (i.e., *variance*). For Rayleigh fading, we found that BVTC-based MREC can attain MRC-like performance and can reduce complexity compared to MRC [1].

For Rician fading and the signal model from (8) the BVTC expression from [1, Eqn. (31)] becomes:

$$\min_{N=1:L} \left[E_s \sum_{i=N+1}^{L} \left(\frac{K\left|h_{\text{d,n},i}\right|^2}{K+1} + \frac{\lambda_i}{K+1} \right) + N_0\, N \right]$$
$$= \min_{N=1:L} \left[E_s \sum_{i=N+1}^{L} \frac{K_i+1}{K+1}\lambda_i + N_0\, N \right] \quad (29)$$

Since K_i, defined in (12), is determined by λ_i as well as by the angle between the channel eigenvector $\mathbf{u}_i$ and the deterministic part of the channel vector $\widetilde{\mathbf{h}}_{\text{d}}$, BVTC for Rician fading requires reordering decreasingly the terms $\lambda_i\,(K_i+1)$, $i = 1 : L$, before (29) is employed to compute the MREC order, N. Note that the BVTC from (29) is independent of the CSI estimation procedure and parameters. Future work will consider a CSI-dependent BVTC implementation.

IV. Numerical Results

A. SIMO Results from AEP Expression

The following parameter settings have been used: QPSK transmitted signal, uniform linear array with $L = 5$ elements and normalized interelement distance $d_{\text{n}} = 1$, mean AOA $\theta_{\text{c}} = 0$, which corresponds to the direction perpendicular to the antenna array, Laplacian PAS with lognormally-distributed AS described by (7), and lognormally-distributed K-factor as described in (6) — unless specified otherwise. SINC and MMSE PSAM have been used for CSI estimation for normalized Doppler speed 0.01, slot length 7, and interpolator size 11 [2]. The results described next have been obtained by the following procedure: 1) Generate a batch of 10 000 independent AS samples from the lognormal distribution (7); its mean and standard deviation are 9.75° and 13.45°, respectively, and Prob(AS $<$ 20°) $=$ 0.84; 2) Generate a batch of 10 000 independent K samples from the lognormal distribution (6) so that AS and K have the required correlation, as discussed in Section II-B; 3) Compute the AEP using (28) for each (AS, K) sample; 4) Compute the mean AEP by averaging over AS and K. Note, however, that for some of the results described hereafter AS or K or both may also be fixed to their average values or other values deemed interesting.

Fig. 1 shows for MMSE PSAM that at mean-AEP 10^{-3}, MRC outperforms BVTC MREC by only about 0.4 dB, but is 10 times more complex. The decorrelating step of MREC allows independent estimation of each eigengain component, which dramatically reduces complexity vs. MRC, for MMSE PSAM. Interestingly, we found that even full-MREC is about 3 times less complex than MRC. Furthermore, at low bit-SNR, BVTC further reduces MREC complexity by reducing the dimension of the estimation and combining problems. On the other hand, BVTC MREC outperforms BF by nearly 7 dB, and doubles the computational complexity vs. the latter.

Fig. 2 shows in the top subplot that, for BVTC MREC, MMSE PSAM outperforms SINC PSAM by almost 2 dB at 10^{-3} mean-AEP, although they have nearly the same complexity [1, Table II]. The bottom subplot indicates that MREC reduces complexity significantly only at low bit-SNR for SINC PSAM because BVTC reduces (estimation and combining) problem dimension. For SINC PSAM, MREC does not simplify eigengain estimation. For Rayleigh fading, similar conclusions have been drawn also by simulation in [7].

Thus, BVTC MREC not only reduces the problem dimension but, more importantly, it can make the great performance of MMSE PSAM affordable. Hereafter, all shown performance results are for BVTC MREC with MMSE PSAM.

Fig. 3 shows in the top subplot that the performance for Rayleigh fading is poor compared to all the Rician fading

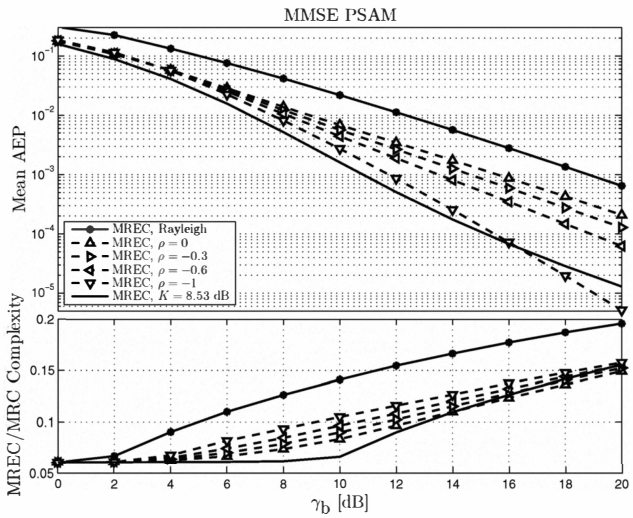

Fig. 1. **Top**: average (over noise, fading, AS and K) error probability vs. bit-SNR, for BF, BVTC MREC and MRC, Rician fading, MMSE PSAM, and $\rho = -0.6$; **Bottom**: BF vs. MREC and MREC vs. MRC relative complexities.

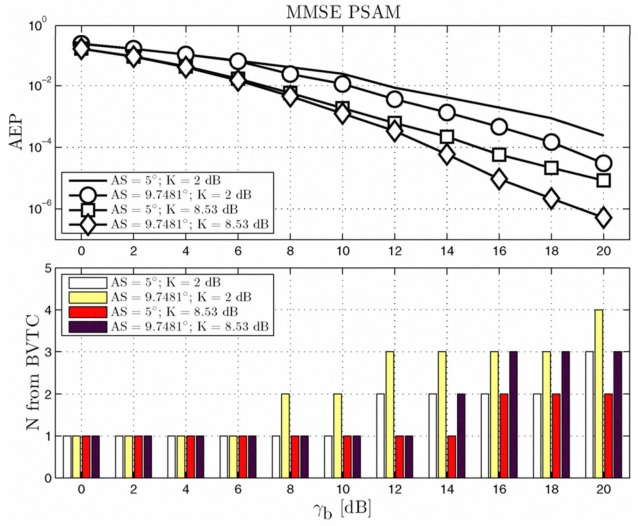

Fig. 2. **Top**: average (over noise, fading, AS and K) error probability vs. bit-SNR, for BVTC MREC, Rician fading with $\rho = -0.6$, SINC and MMSE PSAM; **Bottom**: MREC vs. MRC relative complexity.

cases. On the other hand, for Rician fading with random K, indicated performance improves with increasing AS – K correlation magnitude, $|\rho|$. For example, at mean-AEP level 10^{-3}, Rayleigh fading requires $\gamma_b = 18.75$ dB, whereas Rician fading with $\rho = 0, -0.3, -0.6$ requires 15.6 dB, 14.6 dB, and 13.5 dB, respectively. Finally, Rician fading with $K = 8.53$ dB (the average of the measured distribution) requires only 10.82 dB.

Fig. 3 shows in the bottom subplot that the unrealistic Rayleigh fading assumption overestimates BVTC MREC complexity by about 46% vs. Rician fading with $\rho = -0.6$, at $\gamma_b = 10$ dB. On the other hand, for Rician fading, increasing

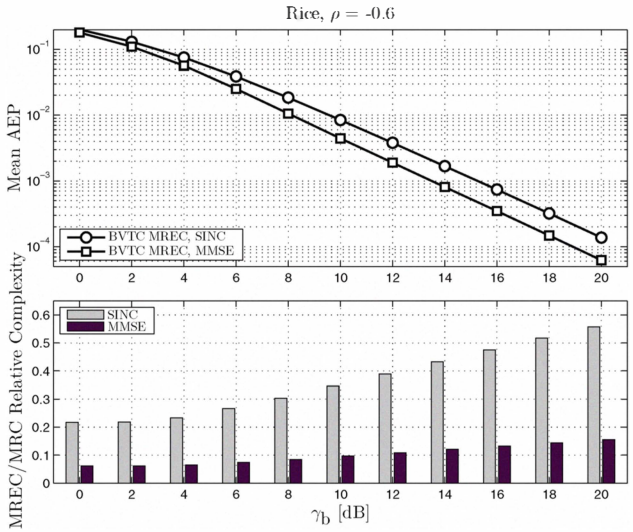

Fig. 3. **Top**: average (over noise, fading, AS and — unless specified otherwise — K) error probability vs. bit-SNR, for BVTC MREC, for Rayleigh and Rician fading, MMSE PSAM, and several AS – K correlation values; **Bottom**: MREC vs. MRC relative complexity. The top subplot legend also applies to the bottom subplot.

$|\rho|$ increases BVTC MREC complexity somewhat — by about 8% and 16% for $\rho = -0.3$ and $\rho = -0.6$, respectively, compared to $\rho = 0$, at $\gamma_b = 10$ dB — because the MREC order output by the BVTC increases. Finally, the unrealistic assumption that K is set to the average from measurements underestimates BVTC MREC complexity by more than 30%, at $\gamma_b = 10$ dB compared to the realistic case of random K with $\rho = -0.6$.

Let us now explore further the reason behind the MREC performance improvement with increasing $|\rho|$. Fig. 4 shows in the top subplot that the AEP performance (averaging over noise and fading only) is high for low AS and low K values. Thus, the (low-AS, low-K) samples determine average performance for random AS and K, which makes the relative number of such samples important. Histograms of (AS, K) shown in Fig. 5 indicate that increasing $|\rho|$ yields relatively fewer (low-AS, low-K) samples. This means relatively fewer poor-performance-inducing samples and, therefore, improved average (over AS and K) performance, as shown in the top subplot of Fig. 3.

Fig. 4 shows in the bottom subplot that, given AS and K, the BVTC order increases with the bit-SNR, which increases the complexity but also helps MREC achieve near-MRC performance. On the other hand, given K, the BVTC order tends to increase with increasing AS, which is because the intended-signal energy is spread over an increasing number of eigenvectors. The top subplot shows a corresponding performance improvement, which is due to diversity gain.

Finally, the top subplot in Fig. 4 indicates that, given the AS, BVTC MREC performance improves with increasing K. This has been confirmed by other numerical results (not shown here due to space limitations). While MREC performance improves with increasing K, its complexity decreases. We found that K

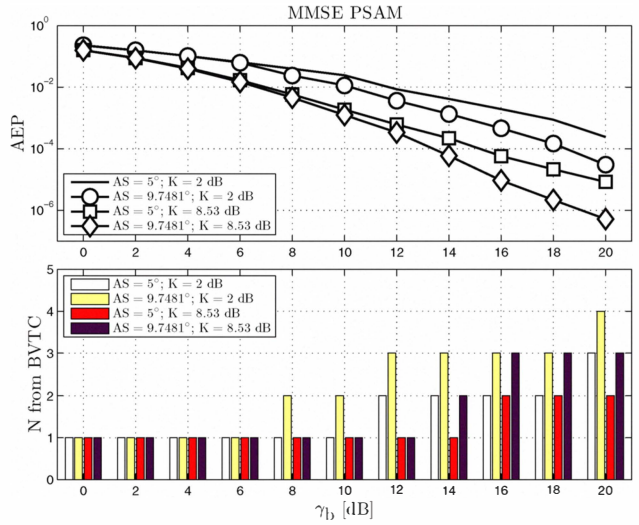

Fig. 4. **Top**: average (over noise and fading only) error probability vs. bit-SNR, for BVTC MREC, Rician fading, MMSE PSAM, and various AS and K values (low or equal to the averages of the distributions described in Section II-B; **Bottom**: MREC order output by the BVTC.

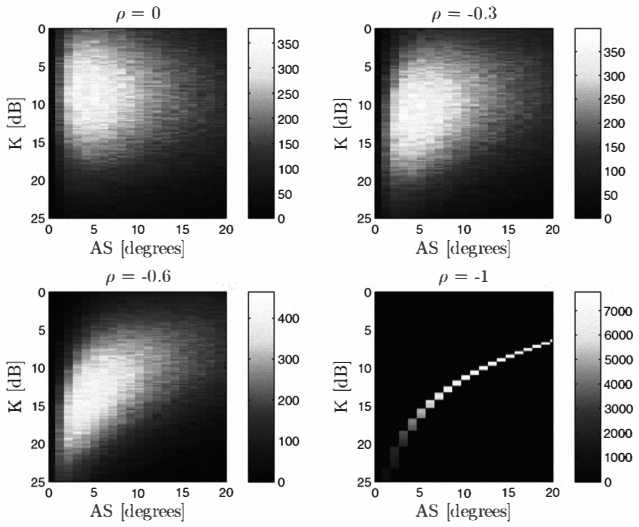

Fig. 5. Histograms of (AS, K) obtained from 10^6 samples, for $\rho = 0, -0.3, -0.6, -1$. Increasing correlation magnitude yields relatively fewer (low-AS, low-K) samples.

increasing from 0 dB to 10 dB would reduce MREC mean-AEP 30 times and MREC complexity by half. On the other hand, the MRC numerical complexity is high and independent of K (as well as AS and bit-SNR).

V. Conclusions

The results obtained above with the newly-derived AEP expression prove that MREC adapted with the proposed criterion to the fading type, AS, K-factor, and SNR can achieve optimum, MRC-like, performance for BF-like complexity (lower than MRC). Computational complexity reductions, i.e., baseband hardware and power savings, are especially attractive (ten-fold) for optimum CSI estimation. Thus, MREC and optimum CSI estimation should be deployed at smart antennas to achieve the full performance permitted by channel conditions for minimum baseband hardware and power cost.

Furthermore, we have found that the fading type and channel parameter models employed in theory or simulation can dramatically impact performance indications and complexity assessments. Recently-validated models of Rician fading with correlated AS and K should be used for performance and complexity evaluations. Assuming Rayleigh fading instead can underestimate performance by about 5 dB at 10^{-3} mean-AEP, and can double the indicated complexity requirements. Assuming Rician fading and typical K value can overestimate performance by nearly 2 dB and can underestimate processing requirements by 30%. Finally, assuming that AS and K are uncorrelated can underestimate achievable performance by 2 dB but does not affect significantly complexity assessments.

MREC proves to be a 'greener' smart antenna technique than BF and MRC because: 1) MREC can significantly reduce complexity for the optimum CSI estimation approach, and 2) MREC can reduce (estimation and combining) problem dimension by adapting to the actual fading parameters (type, AS, K, bit-SNR, etc.).

References

[1] C. Siriteanu and S. D. Blostein, "Maximal-ratio eigen-combining for smarter antenna arrays," *IEEE Transactions on Wireless Communications*, vol. 6, no. 3, pp. 917 – 925, March 2007.

[2] ——, "Maximal-ratio eigencombining: a performance analysis," *Canadian Journal of Electrical and Computer Engineering*, vol. 29, no. 1/2, pp. 15–22, January–April 2004.

[3] A. Paulraj, R. Nabar, and D. Gore, *Introduction to Space-Time Wireless Communications*. Cambridge, UK: Cambridge University Press, 2005.

[4] A. Algans, K. I. Pedersen, and P. E. Mogensen, "Experimental analysis of the joint statistical properties of azimuth spread, delay spread, and shadow fading," *IEEE Journal on Selected Areas in Communications*, vol. 20, no. 3, pp. 523–531, April 2002.

[5] P. Kyosti, J. Meinila, L. Hentila, and *et al.*, "WINNER II Channel Models." CEC, Tech. Rep. IST-4-027756, 2008.

[6] C. Siriteanu, S. D. Blostein, and J. Millar, "FPGA-based communications receivers for smart antenna array embedded systems," *EURASIP Journal on Embedded Systems. Special Issue on Field-Programmable Gate Arrays in Embedded Systems*, vol. 2006, pp. Article ID 81 309, 13 pages, 2006.

[7] C. Siriteanu, G. Xin, and S. D. Blostein, "Performance and complexity comparison of MRC and PASTd-based statistical beamforming and eigencombining," in *Proc. 14th Asia–Pacific Conference on Communications (APCC'08), Tokyo, Japan, Session 16-PM1-A*, 2008.

[8] V. Erceg, P. Soma, D. S. Baum, and S. Catreux, "Multiple-input multiple-output fixed wireless radio channel measurements and modeling using dual-polarized antennas at 2.5 GHz," *IEEE Transactions on Wireless Communications*, vol. 3, no. 6, pp. 2288 – 2298, November 2004.

[9] M. K. Simon and M.-S. Alouini, *Digital Communication over Fading Channels. A Unified Approach to Performance Analysis*. Baltimore, Maryland: John Wiley and Sons, 2000.

[10] C. Siriteanu, Y. Miyanaga, and S. D. Blostein, "Smart antenna performance for correlated azimuth spread and Rician K-factor," in *Proc. 4th International Symposium on Communications, Control and Signal Processing, Limassol, Cyprus, (ISCCSP'10)*, March 2010.